

# Longitudinal broadening of near side jets due to parton cascade

G. L. Ma<sup>1</sup>, S. Zhang<sup>1,2</sup>, Y. G. Ma<sup>1a</sup>, X. Z. Cai<sup>1</sup>, J. H. Chen<sup>1,2</sup>, and C. Zhong<sup>1</sup>

<sup>1</sup> Shanghai Institute of Applied Physics, Chinese Academy of Sciences, P.O. Box 800-204, Shanghai 201800, China

<sup>2</sup> Graduate School of the Chinese Academy of Sciences, Beijing 100080, China

Received: date / Revised version: date

**Abstract.** Longitudinal broadening along  $\Delta\eta$  direction on near side in two-dimensional ( $\Delta\phi \times \Delta\eta$ ) di-hadron correlation distribution has been studied for central Au+Au collisions at  $\sqrt{s_{NN}} = 200$  GeV, within a dynamical multi-phase transport model. It was found that the longitudinal broadening is generated by a longitudinal flow induced by strong parton cascade in central Au+Au collisions, in comparison with p+p collisions at  $\sqrt{s_{NN}} = 200$  GeV. The longitudinal broadening may shed light on the information about strongly interacting partonic matter at RHIC.

**PACS.** 25.75.Nq Quark deconfinement – 25.75.Gz Particle correlations and fluctuations

## 1 Introduction

Di-hadron correlation is thought as a good probe to explore the properties of strongly interacting partonic matter in central Au+Au collisions at the Relativistic Heavy Ion Collider (RHIC) [1]. In di-hadron azimuthal correlations, an away side jet is found quenching and losing its energy into the nearby dense medium, since it has a long interactive path in the medium, i.e. jet quenches [2], which has been supported by many experimental observations such as the medium modification of away side jets in di-hadron azimuthal correlation [3,4]. On the other hand, would a near side jet emitted near the surface be affected by the formation of dense partonic matter? The recently observed longitudinal broadening sitting at a plateau on near side in the  $\Delta\eta$  direction of two-dimensional ( $\Delta\phi \times \Delta\eta$ ) di-hadron correlation function, so-called 'ridge' correlation [5,6,7], is attracting the attentions from theorists (where  $\Delta\phi$  and  $\Delta\eta$  represent the pseudo-rapidity and azimuthal angle differences between the trigger and associated particles), respectively. Chiu and Hwa concluded that it results from enhanced thermal partons by the energy loss of hard partons traversing the bulk medium by using a recombination model [8]. Armesto et al. [9] and Satarov et al. [10] explained it as a consequence of the longitudinal flow of medium created at early stages of a heavy-ion collision. Shuryak argued that the ridge is produced by QCD bremsstrahlung along the beam and then boosted by transverse flow [11]. Majumder and Müller et al. proposed that turbulent color fields caused by plasma instabilities can deflect the transversely propagating partons in the direction of beam axis [12]. Romatschke presented a longitudinal broadening in the frame of elastic

collisional energy loss of heavy quarks in an anisotropic expanding system [13]. Wong simulated the ridge structure by a momentum kick model in which ridge particles are identified as medium partons which suffer collisions with the jet and acquire momentum kicks along the jet direction [14]. However, Pantuev thought it could be the result of the back splash from stopped energetic partons [15]. In this paper, by using a dynamical multi-phase transport model, we found that the longitudinal flow in partonic longitudinal transport process can generate the longitudinal broadening with the evolution of partonic matter in central Au+Au collisions at  $\sqrt{s_{NN}}=200$  GeV, in comparison with the results of p+p collisions at  $\sqrt{s_{NN}} = 200$  GeV.

## 2 Model Introduction

A multi-phase transport model (AMPT) model [16] is a hybrid model which consists of four main processes: the initial conditions, partonic interactions, the conversion from partonic matter into hadronic matter and hadronic interactions. The initial conditions, which include the spatial and momentum distributions of minijet partons and soft string excitations, are obtained from the HIJING model [2]. The parton structure functions are taken as Duke-Owen structure function set 1 [17]. A  $K$  factor of 2.5 has been included to correct the contribution from lowest order pQCD processes. Excitations of strings melt strings into partons. Scatterings among partons are modelled by Zhang's parton cascade model (ZPC) [18], which at present includes only two-body scattering with cross section obtained from the pQCD with screening mass. In the default version of the AMPT model [19](abbr. "the default AMPT" model) partons are recombined with their parent strings when they stop interactions, and the result-

<sup>a</sup> Corresponding author: Email: ygma@sinap.ac.cn

ing strings are converted to hadrons by using a Lund string fragmentation model [20]. In the string melting version of the AMPT model (abbr. “the melting AMPT” model)[21], a simple quark coalescence model is used to combine partons into hadrons. Dynamics of the subsequent hadronic matter is then described by A Relativistic Transport (ART) model [22]. Details of the AMPT model can be found in a recent review [16]. As shown in previous studies about elliptic flow [16,21,23] and Mach cone-like structure [24], the partonic effect can not be neglected in the relativistic heavy-ion collisions. Therefore, the melting AMPT model is much more appropriate than the default AMPT model, especially when the energy density is much higher than the critical density for the QCD phase transition. But in these previous studies with the melting AMPT model [16,21,23,24], parton cascade process does not stop until partons cease to interact, and the hadronization takes place dynamically during the process. It is not reasonable since partonic matter has a limited evolution-time which depends on when the energy density (temperature) of reaction system enters the critical threshold, in a Lattice QCD context [25]. In this study, we tested different evolution-times of partonic matter, after which no partonic interactions are allowed and all left over partons must coalesce into hadrons suddenly. It means that the partonic matter comes to the critical point at a certain time, therefore the evolution-time of partonic matter is comparable with the period during which partons interact. We simulated central Au+Au collisions (0-10% centrality) at  $\sqrt{s_{NN}}=200$  GeV with the melting AMPT model and p+p collisions at  $\sqrt{s_{NN}}=200$  GeV with the default AMPT model. The partonic interacting cross section in the melting AMPT model is taken as 10 mb.

### 3 Analysis Method

Two-dimensional ( $\Delta\phi \times \Delta\eta$ ) di-hadron correlation functions between the trigger and associated hadrons were constructed by a mixing-event technique in our analysis. Here  $\Delta\phi = \phi - \phi_{trig}$  and  $\Delta\eta = \eta - \eta_{trig}$  represents the difference of azimuthal angle and pseudo-rapidity between the trigger and associated particles, respectively. The  $p_T$  window cuts for trigger and associated particles are  $2.5 < p_T^{trig} < 6$  GeV/c and  $1.5 < p_T^{assoc} < 2.5$  GeV/c, respectively. Both trigger and associated particles were selected within pseudo-rapidity window  $|\eta| < 1.0$ . The pairs of the associated particles with trigger particles in the same events were accumulated to obtain a  $\Delta\phi \times \Delta\eta$  distribution. In order to remove the background which is expected to mainly come from the effect of elliptic flow [26, 4], so-called mixing-event method was applied to simulate the background. In this method, we mixed two events which have very close impact parameters (the impact parameter difference of two events is required to be less than 0.5 fm) and the same reaction plane direction into a mixed event, and extracted  $\Delta\phi \times \Delta\eta$  distribution which is regarded as the corresponding background. A zero yield at minimum (ZYAM) assumption [4] was adopted to subtract the background by making the associated yield be

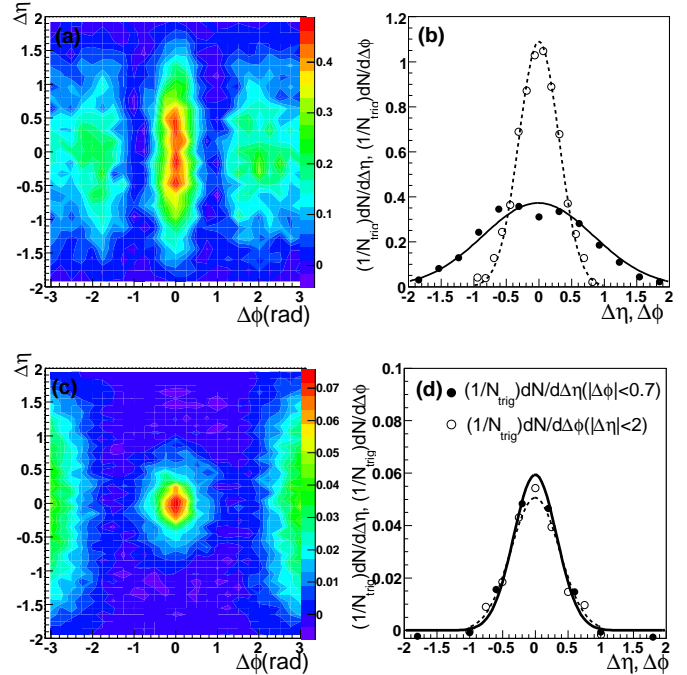


**Fig. 1.** (Color online) Two-dimensional ( $\Delta\phi \times \Delta\eta$ ) di-hadron correlation functions (a) and the projected  $\Delta\eta$  (full circles, within  $|\Delta\phi| < 0.7$ ) and  $\Delta\phi$  (open circles, within  $|\Delta\eta| < 2$ ) distributions of associated hadrons (b) on near side for central Au+Au collisions (0-10%) in the melting AMPT model with hadronic rescattering; (c) and (d): The corresponding ones for p+p collisions at  $\sqrt{s_{NN}}=200$  GeV in the default AMPT model with hadronic rescattering. The lines in (b) and (d) are the Gaussian fitting functions to the  $\Delta\eta$  (solid) and  $\Delta\phi$  (dash) projections.

zero around  $|\Delta\phi|=1$  (i.e. the strip of  $0.9 < |\Delta\phi| < 1.1$ ) after subtraction.

### 4 Results

Figure 1(a) and (c) give the background subtracted two-dimensional ( $\Delta\phi \times \Delta\eta$ ) di-hadron correlation functions for central Au+Au collisions (0-10%) at  $\sqrt{s_{NN}}=200$  GeV in the melting AMPT model with hadronic rescattering and p+p collisions at  $\sqrt{s_{NN}}=200$  GeV in the default AMPT model with hadronic rescattering, respectively. A significant longitudinal broadening in the  $\Delta\eta$  direction on near side ( $|\Delta\phi| < 1.0$ ) is observed in central Au+Au collisions, as compared to that in p+p collisions. Figure 1(b) and 1(d) gives the projected  $\Delta\eta$  (within  $|\Delta\phi| < 0.7$ ) and  $\Delta\phi$  (within  $|\Delta\eta| < 2$ ) distributions of associated hadrons for near side in Au+Au and p+p collisions respectively, where the solid and dash lines give the corresponding Gaussian fitting functions. As a result, the ratio between two root mean squares of the projected  $\Delta\eta$  and  $\Delta\phi$  distributions (i.e.  $\text{rms}(\Delta\eta)/\text{rms}(\Delta\phi)$ ) was found to be  $\sim 2.6$  in central Au+Au collisions, but  $\sim 1.0$  in p+p collisions, which is consistent with the preliminary experimental observation [5] and theoretical calculation [13].

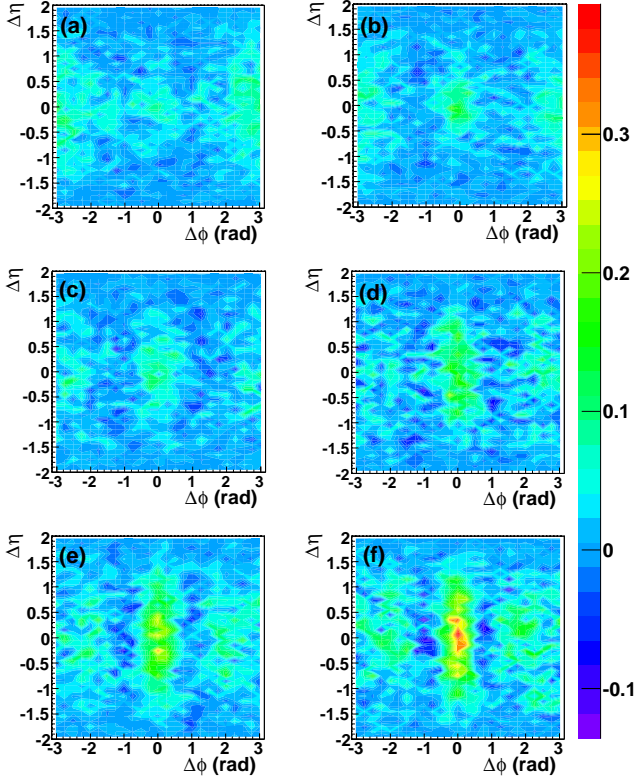


**Fig. 2.** (Color online) Two-dimensional ( $\Delta\phi \times \Delta\eta$ ) di-hadron correlation functions with different evolution-times of partonic matter in central Au+Au collisions (0-10%) at  $\sqrt{s_{NN}}=200$  GeV in melting AMPT model without hadronic rescattering. (a): 0.5 fm/c; (b): 1.0 fm/c; (c): 1.5 fm/c; (d): 2.5 fm/c; (e): 3.0 fm/c; (f): 4.0 fm/c.

In order to learn about the evolution of longitudinal broadening in the parton cascade processes for central Au+Au collisions, Fig. 2(a)-(f) presents the two-dimensional ( $\Delta\phi \times \Delta\eta$ ) di-hadron correlation functions with different evolution-times of partonic matter, where the effect of hadronic rescattering is found to be negligible in the study. As seen from figure 2 (a) and (b), no obvious broadening is seen in the longitudinal  $\Delta\eta$  direction with a short evolution-time. But the longitudinal broadening emerges and grows up with the evolution-time ((c)-(f)), which indicates strong and continuous parton cascade processes broaden the  $\Delta\eta$  distribution of the associated particles on near side longitudinally. On the other hand, near side seems unchanged with partonic evolution-time in shape in the  $\Delta\phi$  direction.

Quantitatively, figure 3 (a) and (b) give the evolution-time dependences of rms( $\Delta\eta$ ) and the integrated yield for near side within  $|\Delta\phi| < 0.7$  in central Au+Au collisions (0-10%) at  $\sqrt{s_{NN}} = 200$  GeV, respectively, where the final hadronic rescattering has not been included. Because p+p collisions are thought to rarely experience the processes of parton cascade commonly, the results of p+p collisions at  $\sqrt{s_{NN}} = 200$  GeV are plotted at zero evolution-time for the reference. From figure 3(a), it is apparent that the rms( $\Delta\eta$ ) of near side increases and saturates with the

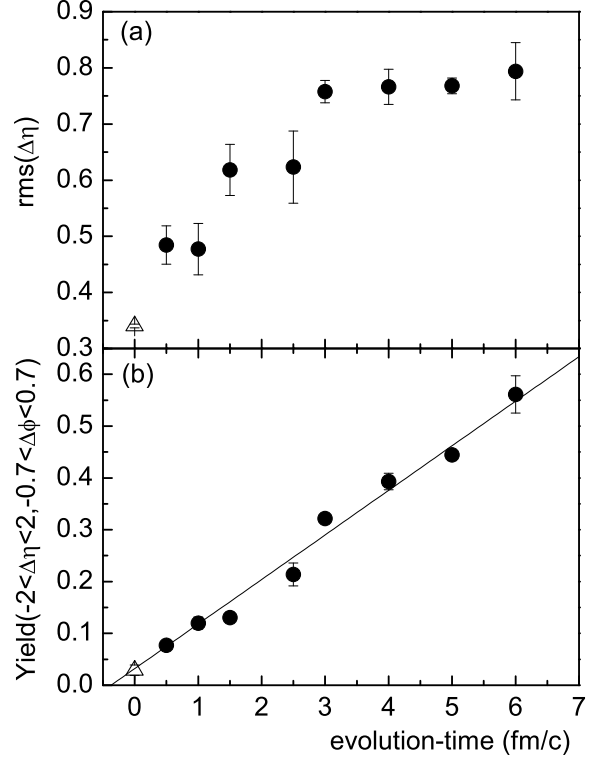


**Fig. 3.** Full circles: the evolution-time dependences of rms( $\Delta\eta$ ) (a) and integrated near side yield within  $|\Delta\phi| < 0.7$  (b) in Au+Au collisions at  $\sqrt{s_{NN}}=200$  GeV in the melting AMPT model without hadronic rescattering; Open triangles: the corresponding values in p+p collisions at  $\sqrt{s_{NN}}=200$  GeV without hadronic rescattering; Solid line in (b) shows a linear fitting function, see the text for the detail.

evolution-time of partonic matter. It can also be seen in figure 3(b), the associated near-side yield per trigger particle seems to increase linearly with the evolution-time (the slope =  $0.085 \pm 0.002 \text{ fm}^{-1}$ ), which is consistent with our previous work [27].

## 5 Discussions

To investigate partonic longitudinal transport process in central Au+Au collisions, figure 4 (a) presents the pseudo-rapidity distributions of partons at different partonic evolution-times in central Au+Au collisions at  $\sqrt{s_{NN}} = 200$  GeV. We used a non-uniform longitudinal flow model (NUFM) [28] to fit these partonic pseudo-rapidity distributions from AMPT model, as shown by the lines in figure 4 (a). As a consequence, two fitting parameters (i.e. ellipticity  $e$  (circles) and rapidity limit  $\eta_{e0}$  (squares)) as a function of the evolution-time of partonic matter are gotten in figure 4 (b). The ellipticity, which represents the uniformity of fireball in the longitudinal direction, drops until 3.0

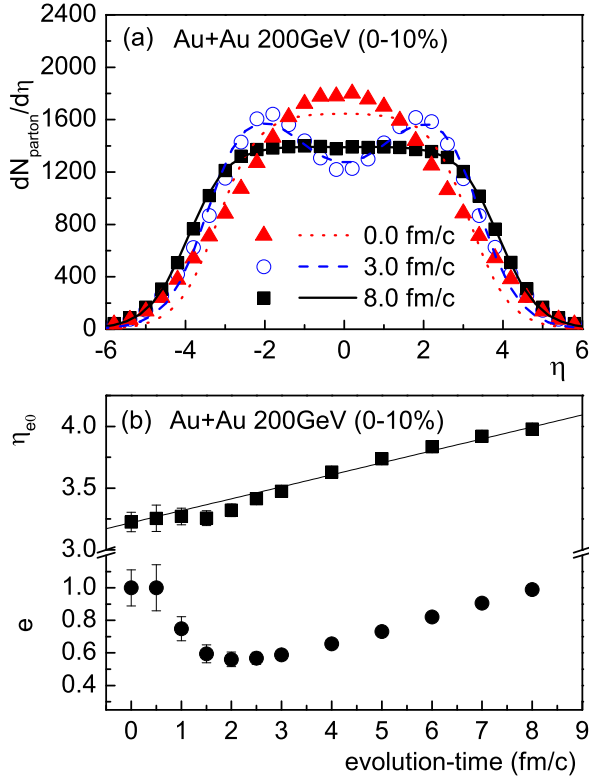


**Fig. 4.** (Color online) (a) The pseudo-rapidity ( $\eta$ ) distributions of partons with three different evolution-times of partonic matter in Au+Au collisions at  $\sqrt{s_{NN}}=200$  GeV in the melting AMPT model (points), where the lines shows the fits from NUFM model which is defined in the text and Ref. [28]; (b) The ellipticity  $e$  (circles) and the rapidity limit  $\eta_{e0}$  (squares), from NUFM fits to the  $\eta$  distributions of partons, as a function of the evolution-time of partonic matter in Au+Au collisions at  $\sqrt{s_{NN}}=200$  GeV in the melting AMPT model, where solid line shows a linear fitting function.

fm/c firstly and then increases with the evolution-time, which implies the scenario that the longitudinal evolution starts from the superposition of projectile and target systems, and they penetrate each other and diffuse via further parton interactions. On the other hand,  $\eta_{e0}$ , which represents the amplitude of longitudinal flow, increases with evolution-time almost linearly (the slope =  $0.093 \pm 0.003$   $fm^{-1}$ , which is consistent with that of the associated near-side yield shown in figure 3(b)). Therefore, the existence of strong partonic longitudinal flow can result in the above observed elongated structure in the  $\Delta\eta$  direction.

In Ref [8], a hard parton near surface was predicted to lose some amount of energy to enhance thermal motion of the partons in the environment, which was expected to result in the longitudinal broadening of near side in central Au+Au collisions at RHIC energy. However it has not given the dynamical detail about how a hard parton losses its energy into the medium. In Ref [13], Romatschke dis-

cussed the collisional energy loss of hard parton is in favor of the production of the longitudinal broadening, but in the frame of heavy quarks. In the present work, we found that the longitudinal broadening can be produced by the longitudinal flow induced by parton cascade longitudinally, by using a dynamical multi-phase transport model. On the other hand, we presented the width of longitudinal broadening ( $rms(\Delta\eta)$ ) increases with the evolution-time of partonic matter, which is consistent with the conclusion in Ref [10] that the width of elongated structure is proportional to the logarithmic 'formation time' of near side correlation for a longitudinally-expanding QGP with a constant sound velocity.

Recently, three-particle  $\Delta\eta$  correlation is expected to play a role to identify the possible physical mechanisms on 'ridge' [29], and our corresponding work is in progress. Though the plateau of 'ridge' correlation is not observed in our model, our present work has provided one possibility to interpret longitudinal broadening (i.e. induced by strong parton cascade) on near side which was observed in central Au+Au collisions at RHIC energy.

## 6 Summary

To summarize, we have explored the origin of longitudinal broadening on near side in central Au+Au collisions at RHIC energy within the framework of multi-phase transport model. In comparison with p+p collisions, it has been found that the longitudinal broadening in central Au+Au collisions is driven by the longitudinal flow induced by strong parton cascade. Therefore the researches on longitudinal broadening can give more information about early partonic stage in relativistic heavy ion collisions.

Authors thank Prof H. Z. Huang for the discussion. This work was supported in part by the National Natural Science Foundation of China under Grant No 10610285 and 10705044, and the Knowledge Innovation Project of Chinese Academy of Sciences under Grant No. KJXC2-YW-A14 and KJXC3-SYW-N2, the Startup Foundation for the CAS Presidential Scholarship Award under Grant No. 29010702.

## References

1. I. Arsene et al. (BRAHMS Collaboration), Nucl. Phys. A **757**, (2005) 1; B. B. Back et al. (PHOBOS Collaboration), Nucl. Phys. A **757**, (2005) 28; J. Adams et al. (STAR Collaboration), Nucl. Phys. A **757**, (2005) 102; S. S. Adler et al. (PHENIX Collaboration), Nucl. Phys. A **757**, (2005) 184.
2. X.-N. Wang and M. Gyulassy, Phys. Rev. D **44**, (1991) 3501; M. Gyulassy and X.-N. Wang, Comput. Phys. Commun. **83**, (1994) 307.
3. C. Adler et al. (STAR Collaboration), Phys. Rev. Lett. **90**, (2003) 082302.
4. S. S. Adler et al. (PHENIX Collaboration), Phys. Rev. Lett. **97**, (2006) 052301.
5. P. Jacobs, Eur. Phys. J. C **43**, (2005) 467.

6. J. Adams et al.(STAR Collaboration), Phys. Rev. Lett. **95**, (2005) 152301.
7. Jörn Putschke (for the STAR Collaboration), J. Phys. G **34**, (2007) S679, Proc QUARK MATTER 2006, Shanghai, eds. Y. G. Ma, E. K. Wang, X. Cai, H.Z. Huang, X. N. Wang and Z. Y. Zhu.
8. C. B. Chiu and R. C. Hwa, Phys. Rev. C **72**, (2005) 034903.
9. Néstor Armesto, Carlos A. Salgado, and Urs Achim Wiedemann, Phys. Rev. Lett. **93**, (2004) 242301.
10. L. M. Satarov, H. Stöcker and I. N. Mishustin, Phys. Lett. B **627**, (2005) 64.
11. E. Shuryak, Phys. Rev. C **76**, (2007) 047901.
12. A. Majumder, Berndt Müller, and Steffen A. Bass, Phys. Rev. Lett. **99**, (2007) 042301.
13. P. Romatschke, Phys. Rev. C **75**, (2007) 014901.
14. Cheuk-Yin Wong, Phys. Rev. C **76**, (2007) 054908.
15. V. S. Pantuev, arXiv:0710.1882.
16. Z. W. Lin, C. M. Ko, B. A. Li, B. Zhang, S. Pal, Phys. Rev. C **72**, (2005) 064901.
17. D.W. Duke and J.F. Owens, Phys. Rev. D **26**, (1982) 1600.
18. B. Zhang, Comput. Phys. Commun. **109**, (1998) 193.
19. B. Zhang, C. M. Ko et al., Phys. Rev. C **61**, (2000) 067901.
20. B. Andersson, G. Gustafson et al., Phys. Rep. **97**, (1983) 31.
21. Z. W. Lin, C. M. Ko, Phys. Rev. C **65**, (2002) 034904; Z. W. Lin, C. M. Ko et al., Phys. Rev. Lett. **89**, (2002) 152301.
22. B. A. Li and C. M. Ko, Phys. Rev. C **52**, (1995) 2037 .
23. J. H. Chen, Y. G. Ma, G. L. Ma et al., Phys. Rev. C **74**, (2006) 064902.
24. G. L. Ma, S. Zhang, Y. G. Ma et al., Phys. Lett. B **641**, (2006) 362 ;  
G. L. Ma, Y. G. Ma, S. Zhang et al., Phys. Lett. B **647**, (2007) 122;  
G. L. Ma, S. Zhang, Y. G. Ma, J. Phys. G **34**, (2007) S693, Proc QUARK MATTER 2006, Shanghai, eds. Y. G. Ma, E. K. Wang, X. Cai, H.Z. Huang, X. N. Wang and Z. Y. Zhu.
25. F. Karsch and E. Laermann, arXiv:hep-lat/0305025.
26. J. Adams et al. (STAR Collaboration), Phys. Rev. Lett. **95**, (2005) 152301.
27. G. L. Ma, S. Zhang, Y. G. Ma et al., arXiv:nucl-th/0610088.
28. Feng Shengqin, Liu Feng, Liu Lianshou, Phys. Rev. C **63**, (2000) 014901.
29. Pawan Kumar Netrakanti (for the STAR Collaboration), arXiv:0804.4417.